Draft version January 12, 2016
Preprint typeset using LaTeX style emulateapj v. 12/16/11

THE IMPLICATIONS OF THE MAGELLANIC CLOUDS FOR THE FORMATION THE MILKY WAY SYSTEM

Yu Lu[1], et al.

Draft version January 12, 2016

ABSTRACT

The Large and Small Magellanic Clouds (LMC/SMC) are significant companions of the Milky Way galaxy and provide useful information about the formation of the Milky Way. By analyzing a suite of high-resolution N-body simulations of Milky Way-sized host halos and semi-analytic model predictions, we find that the existence of the LMC/SMC-like companions strongly correlates with the formation history and the concentration of the host halo. We explore the parameter space of a flexible semi-analytic galaxy formation model with Markov-Chain Monte-Carlo and find that ignoring the prior knowledge about the host properties that are correlated with the existence of the LMC/SMC can lead to a biased inference for galaxy formation physics. In particular, when the galaxy formation model is calibrated to reproduce the observed stellar mass for Milky Way satellite galaxies, different host halos are found to require different levels of feedback strength, leaving imprints on the mass-metallicity relation of dwarf galaxies and the number counts of lower mass satellite galaxies that are accreted with the LMC/SMC. The results suggest that accurate modeling of the metallicity relation and accretion history of higher-order satellite galaxies play a key role in further tightening the constraints on the formation of the Milky Way system.

1. INTRODUCTION

Our own galaxy, the Milky Way galaxy, provides an excellent laboratory for constraining cosmology and galaxy formation physics. These studies require accurate models for the formation of galaxies and the host halo to make meaningful comparisons between theory and observation. Conventionally, a Milky Way host halo is defined by a given present-day mass, but the importance of properties other than mass when selecting Milky Way (MW) analogues has been realized in recent studies (e.g Busha et al. 2011b). For instance, it has been shown that the concentration of the MW halo is also an important parameter when matching simulated MWs and observations (Mao et al. 2015). We investigate in this paper the implications of the existence of high-mass satellite galaxies, the Large and Small Magellanic Clouds (LMC/SMC), for understanding the formation of the MW system.

The LMC and SMC are significant members of the satellite system of the MW. Both of them are measured to have maximum circular velocities $V_{\rm max} \geq 60{\rm kms}^{-1}$ with magnitudes $M_{\rm v} = -18.5$ and -17.1, respectively (van der Marel et al. 2002; Stanimirović et al. 2004; van den Bergh 2000; van der Marel & Kallivayalil 2014). The next brightest satellite is Sagittarius, about 4 magnitudes dimmer, with $V_{\rm max} \sim 20{\rm kms}^{-1}$ (Strigari et al. 2007). In terms of stellar mass, the LMC and SMC have significantly higher stellar masses than the rest of the MW satellite galaxy population. The stellar mass of the LMC is about $1.5\times10^9{\rm M}_\odot$, and the stellar mass of the SMC is about $4.6\times10^8{\rm M}_\odot$, which are 1.8 and 1.3 dex higher than the stellar mass of Sagittarius dSph, which is $2.1\times10^7{\rm M}_\odot$ (McConnachie 2012). This difference is often referred as MW satellite galaxy mass gap (e.g. Cautun et al. 2014a; Jiang & van den Bosch 2015). For the rest of the satellite population, the differences between two sequential galaxies are no larger than 0.5 dex (the 5th and the 6th). These distinct features make the LMC/SMC special in the MW satellite population. The significance of the the LMC and SMC as major satellites of the MW and their implications have been discussed in the literature from both theoretical and observational point of view by many authors.

There have been theoretical studies in the literature investigating the implications of high-mass substructures in the MW analogues. Busha et al. (2011b) have studied the likelihood that MW-like systems host massive satellite galaxies. They assumed a certain host halo mass for the MW and applied a sub halo abundance matching model (SHAM) to study the statistics for the MW to host LMC/SMC. They found that MW-like objects in their selection had a 5%–11% chance to host two subhalos as large or as luminous as the SMC with relevant properties, including their circular velocity, distance from the center of the MW, and velocity within the MW halo, in agreement with previous simulation results (e.g. Boylan-Kolchin et al. 2010). In Busha et al. (2011a), the authors matched the stellar masses of the satellite population using a SHAM and asked what the implications were for the properties of the host halo, including its mass. They constrained the MW virial mass, $1.2^{+0.7}_{-0.4}$ (stat.)$\pm$0.3 (sys.) $\times10^{12}{\rm M}_\odot$ (68% confidence). In addition, they also calculated the probability distribution for the density profile of the MW and its satellite accretion history, and found that although typical satellites of $10^{12}{\rm M}_\odot$ halos are accreted over a wide range of epochs over the last 10 Gyr, a ∼72% probability that the LMC and SMC were accreted within the last Gyr, and a 50% probability that they were accreted together. In recent studies, Mao et al. (2015) and Wang et al. (2015) demonstrated the need to consider the dependence of satellite occupation on concentration when inferring the mass or other properties of the MW halo from satellites. These studies, however, are limited to the dark matter skeleton of the MW system.

[1] The Observatories, The Carnegie Institution for Science, 813 Santa Barbara Street, Pasadena, CA 91101, USA

The baryonic processes of galaxy formation are known to significantly impact the satellite galaxy population (Benson et al. 2002a,b). A number of authors have adopted various approaches to model the formation of MW satellite galaxies. Koposov et al. (2009) used a number of toy models to add galaxy properties to dark matter halos generated using a combination of Press-Schechter theory with semi-analytic models for tracking subhalo orbits (Zentner et al. 2005). They found that it was very difficult to model objects as bright as LMC and SMC without allowing for an extremely high star formation efficiency. This finding extended the underprediction of high-mass subhalos to an underprediction of luminous satellites, implying that the MW system is unusual owing to the existence of LMC/SMC. Similarly, Okamoto et al. (2010) explored a range of feedback models to add galaxies to some of the high-resolution Aquarius halos (Springel et al. 2008), and again found it difficult to readily reproduce halos with luminosities as bright as the MCs when the luminosities of lower mass satellite galaxies are matched.

While this difficulty could stem from wrong physics being considered in current galaxy formation models, it is possible that the influence of the underlying dark matter structure causes the issue. As the backbone of galaxy formation, the dark matter halo and its associated subhalos impose important constraints on the properties of galaxies that form in them. It is widely acknowledged that the formation history, number of substructures, and environment can affect galaxy formation. Thus, to accurately model the formation of a particular galaxy, for instance the Milky Way, requires prior knowledge about the host dark matter halo. Moreover, one has to admit that current galaxy formation models are premature. Even for a well defined galaxy formation model, large uncertainties still exist, and need to be constrained using observational data. One needs to exhaustively explore the parameter space to identify "successful" models to interpret the physics of galaxy formation in a meaningful way.

This paper is dedicated to investigating the host halo prior. We try to gain insight into what halo properties are of interests when modeling the formation of MW satellite galaxies. To achieve this, we study a set of N-body simulations of MW-sized halos, and apply a semi-analytic model on the merger trees extracted from those simulations to study the galaxy properties. Furthermore, to understand how halo priors influence inferences of galaxy formation physics, we employ a MCMC machinery that is joint with our SAM to explore the parameter space of galaxy formation. We investigate the effect of halo prior and gain insight into what aspects of modeling and observational work are needed to further tighten the constraints on the formation of MW satellite galaxies. Using the posterior probability distribution obtained with MCMC, we will make full predictions for the metallicity relation satellite galaxies and the mass function of higher order satellites in the MW. We explore the parameter space to understand the constraining power of the these observations to shed light on future theoretical studies.

In this paper, we describe the simulations and the modification of the SAM we use in §2. The results we obtain in this study are presented in §3. We summarize the conclusions of the study and discuss the implications in §4.

2. METHODOLOGY

2.1. *The simulations*

In this study, we use two sets of N-body simulations, a cosmological simulation of c125-2048 (Matthew R. Becker in prep) and a suite of high-resolution zoom-in simulations of halos with similar final masses (Mao et al. 2015). The c125-2048 simulation is a dark matter-only cosmological simulation run with 2048^3 particles and a side length of $125\mathrm{Mpc}h^{-1}$, particle mass of $1.8 \times 10^7\mathrm{M}_\odot h^{-1}$, started at $z = 199$. The softening length is $0.5\mathrm{kpc}h^{-1}$, constant in comoving length. The cosmological parameters are $\Omega_\mathrm{M} = 0.286$, $\Omega_\Lambda = 0.714$, $h = 0.7$, $\sigma_8 = 0.82$, and $n_s = 0.96$. We select all the halos that have virial mass $M_\mathrm{vir} = 10^{12.1\pm0.03}\mathrm{M}_\odot$ at $z = 0$, which yields a large sample ~ 1300 halos. The zoom-in simulations consist of 46 halos with final mass in the same mass range selected from a lower resolution sister simulation c125-1024. The parameters and initial conditions of these two boxes are identical, but c125-1024 contains 1024^3 particles and starts at a different redshift, $z = 99$. The mass of the high-resolution particles in the zoom-in simulations is $3.0 \times 10^5\mathrm{M}_\odot h^{-1}$. The softening length in the highest-resolution region is $170\mathrm{pc}h^{-1}$ comoving. Out of the 46 halos, we adopt 38 of them for the studies in this paper and discard 8 others because they include a very large lagrangian volume making the MCMC-SAM calculation practically intractable. For a detailed description of these simulations, including halo identification and merger tree construction, readers are referred to Mao et al. (2015).

With these simulated dark matter halos, we first study the mass accretion histories (MAHs) of MW halos. The MAH is defined as the virial mass of the main-branch halo as a function of redshift or time (Springel et al. 2005). Figure 1 shows the MAH of three randomly selected host halos from the simulations. For each halo in the zoom-in simulation, we identify the same halo from the c125-2048 simulation by matching the location. The figure shows that the host MAHs from the two simulations with different mass resolutions are very similar within the mass resolution limit of the c125-2048 simulation. Tasitsiomi et al. (2004) proposed a 2-parameter model, which combines the exponential model (Wechsler et al. 2002) and the power-law model van den Bosch (2002), to describe a halo MAH. The model is

$$M(z) = M_0 \left(\frac{1+z}{1+z_0}\right)^{-\beta} \exp\left[-\gamma(z-z_0)\right]. \qquad (1)$$

Using this model, McBride et al. (2009) fit the MAHs of halos in the Millennium simulation in a large halo mass range, and found that the 2-parameter model remarkably well captures the halo MAHs. Following the previous work, we also fit the MAHs of the MW halos in our simulations using this model. We overplot the best fit model in Figure 1 for the three examples. As one can see, the overall shape of the MAHs is well captured by the best fit model. We also show how the best-fit parameters for the MAHs from high-res and low-res simulations compare in Figure 2. The fitting parameters are in general agreement. We point out that a merit of this

fitting model is that the model parameters characterize the accretion rate of a halo at early and late epochs. In this model, we find that

$$\frac{\mathrm{d}\log M}{\mathrm{d}z} = -\left(\frac{\beta}{1+z}+\gamma\right), \quad (2)$$

and

$$\frac{\mathrm{d}\log M}{\mathrm{d}\log a} = \beta+\gamma(1+z). \quad (3)$$

The derivation indicates that at the present time, when z=0 and $a=1$, the accretion rate $\mathrm{d}\log M/\mathrm{d}\log a$ is $\beta+\gamma$, and at early times, the accretion rate is more characterized by parameter γ. Motivated by these indications, we will use $\beta+\gamma$ and γ extracted from the best-fit model to characterize halo accretion rates at late and early times for each halo, and to study the correlation between the MAH and the satellite population.

We also measure the concentration parameter of the simulated host halos. The median concentration of the large low-resolution sample is $c_{\rm median}=11.5$. The concentrations predicted for the counterparts in the high-resolution and the low-resolution simulations do not always agree, especially the low-concentration ones. Halos with low concentration in the low-resolution run tend to show large deviation in their concentration parameter. This is different from the MAH fitting parameters, which seem to agree much better between the two sets of the simulations. In this study, we will use both simulations, taking advantage of the large number of halos from the low-resolution simulation for better statistics and the high mass resolution from the zoom-in simulation.

2.2. *The SAM and an approximation scheme for predicting the satellite population*

To study the baryonic component of MW satellites, we adopt the SAM developed by Lu et al. (2011, 2014) and apply the model to the merger trees extracted from the high-resolution zoom-in simulations. Because the simulation has very high mass and time resolution, the merger trees have a large number of branches that end up with a satellite galaxy below mass range of interest in this study. Therefore, following the full tree in a SAM calculation is inefficient for this study and prohibits efficient parameter space exploration. To allow exhaustive parameter space exploration, we adopt a scheme in the SAM to speed up the SAM calculation by ignoring satellite galaxies that are significantly below the lower mass limit of interests. In the scheme, we focus the computation only on the subhalos that are still present at $z=0$, but ignore the subhalos that are accreted into the final host too early to survive until the present day. The high mass resolution of the simulation guarantees that the stellar mass of the satellite galaxies produced in the ignored branches would be much lower than our interests in a sensible model. We note that subhalos that are accreted into branches other than the main branch of the MW host are not ignored in this scheme even though they have been disrupted by the present time, because they can affect the evolution of the satellite galaxies we are interested in at $z=0$. We have compared the stellar masses of the satellite galaxies predicted using the new scheme and the full SAM. We find that $<4\%$ of the satellites down to $M_*=10^4\mathrm{M}_\odot$ are predicted with a deviation in the stellar mass larger than 2% for all the zoom-in simulation merger trees. We conclude that the new scheme accurately reproduces the stellar masses of all satellites in the mass range of this study. We therefore adopt the scheme in this study. This scheme typically reduces the computation time by a factor of 4 for each MW merger tree. The benefit in speeding up the calculation allows us to use MCMC to sample the posterior distribution of the model under data constraints of the MW satellite stellar mass function.

2.3. *Likelihood function for Milky Way satellite galaxy stellar mass function*

To conduct a Bayesian inference from the MW satellite mass function, we need to write down the likelihood function of the model. The data we use in this paper is the stellar mass function of the MW satellite galaxies, down to the 11^{th} most massive satellite galaxy ($M_*=2.9\times10^5\mathrm{M}_\odot$). Tollerud et al. (2008) have shown that incompleteness of MW satellite galaxy count becomes important only for faint dwarfs $M_v>-7$ or $L>10^5L_\odot$. The data we are using should not suffer from incompleteness, so we do not include any treatment to account for survey incompleteness for our model prediction. The theoretical prediction for the mass function is straightforward, but the likelihood function of the satellite mass function is unknown. Poisson probability distribution is a model one would consider, but Boylan-Kolchin et al. (2010) found that the Poisson distribution does not accurately describe the distribution function of subhalo mass function predicted by N-body simulation. Similar findings have also been reported in independent studies (e.g. Busha et al. 2011a; Cautun et al. 2014b). In a recent paper, Mao et al. (2015) argued that the deviation from Poisson can be largely attributed to the effect of varying concentration for a fixed halo mass. To choose an accurate model for the distribution function of the satellite galaxies predicted by a model, we apply a fiducial SAM to the merger tree set. Taking advantage of the large sample of the low-resolution MW simulation set, we study the distribution of the predicted mass function for modeling the likelihood function.

The fiducial model we use here was tuned to match the field galaxy stellar mass function of the local Universe (Lu et al. 2014). We apply the model to the low-resolution merger trees to make a prediction for the MW satellite population. For each merger tree, we extract the subhalo mass function from the N-body simulation itself, and predict the satellite stellar mass function using the fiducial SAM. In Figure 3, we show the subhalo mass function on the left panel and the SAM predicted satellite stellar mass function on the right panel. The blue box extends horizontally from the lower to upper quartile values of the mass of i^{th} subhalo (satellite), with a middle line indicating the median of the mass distribution. The whiskers extend from the box to show the range of the mass in the sample. On the other hand, the gray shaded region covers the 1-σ range of the accumulative distribution function $N(>M)$ as a function of $\log M$. In comparison, we also show the expected 1-σ scatter of the mass function assuming it is Poisson distributed with red vertical error bars. By eye, the expected Poisson errors roughly match the simulation predicted standard deviation (gray shaded region). Nevertheless, we will show later that the real distribution of the mass functions

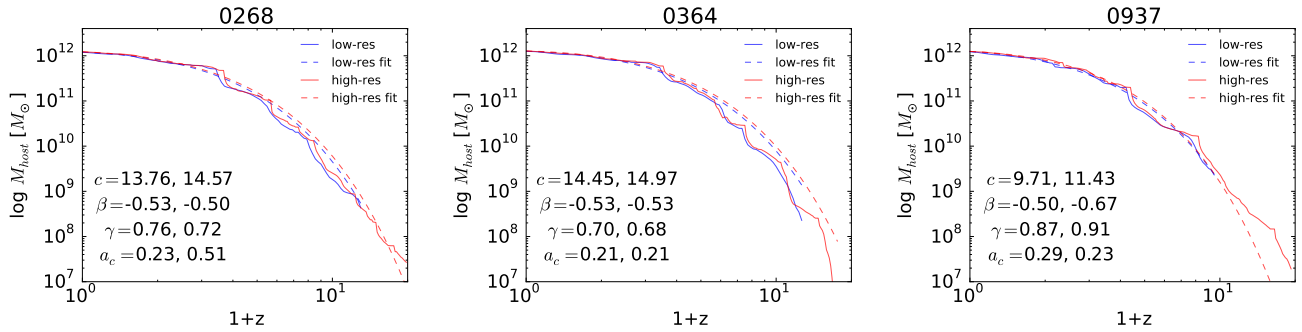

FIG. 1.— The halo mass accretion histories of three typical host halos. The blue solid line denotes the MAH predicted by the low-res c125-2048 simulation, and the solid red line denotes the MAH of the same halo predicted by the high-res zoom-in simulation. The dashed lines with same color denote the corresponding fitting model using Eq.1. The halo concentration and fitting parameters are listed in each panel. The first column is for the low-res halo, and the second column is for the high resolution counterpart.

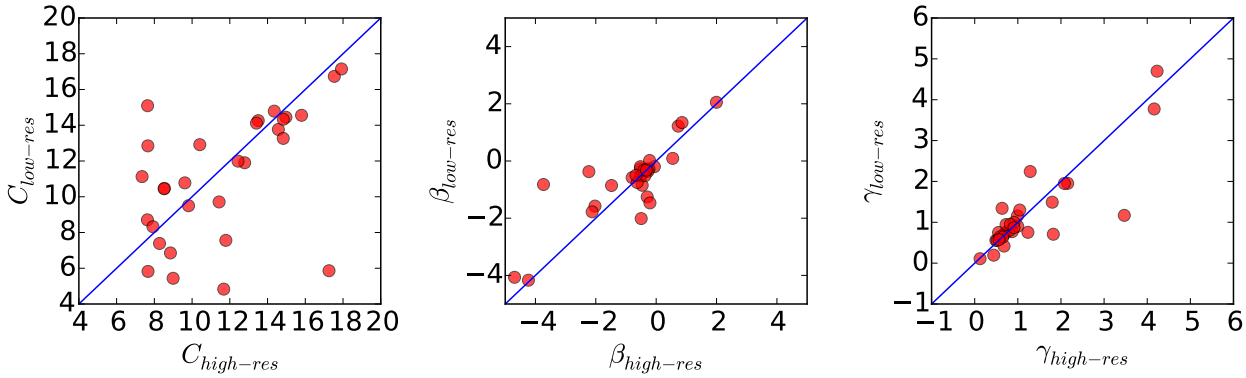

FIG. 2.— We compare the parameters low-resolution and high-resolution host halos. Left panel: the concentration parameter predicted in the high-res simulation and in the low-res simulation for same halos. Middle panel and right panel shows the comparisons of the fitting parameters for the host halo mass accretion history.

quantitatively deviates from Poisson. Moreover, we also overplot the observed MW satellites in the right panel. Without further tuning the model against the data, the fiducial model prediction is in a good agreement with the data, with all the data points covered by the $1-\sigma$ region of the predicted distribution.

The probability distribution function of the number count of subhalos is found to be better described by the Negative Binomial Distribution (NBD) (Boylan-Kolchin et al. 2010),

$$P(N|r,p) = \frac{\Gamma(N+r)}{\Gamma(r)\Gamma(N+1)} p^r (1-p)^N \,, \qquad (4)$$

where N is the number of subhalos per host, $\Gamma(x) = (x-1)!$ is the Gamma function, and r and p are two parameters in the NBD. This distribution function has also been used to describe the probability of the number of satellite galaxies in HOD models (e.g. Berlind & Weinberg 2002). Boylan-Kolchin et al. (2010) found that this distribution function describes the probability distribution of subhalo mass function more accurately than the Poisson distribution because it captures a small fraction of intrinsic non-Poisson scatter of the mass function. The authors defined a parameter $s_{\rm I} = \frac{\sigma_{\rm I}}{\mu}$, the fractional scatter from the intrinsic scatter, $\sigma_{\rm I}$, with respect to the Poisson scatter, μ. The two parameters in the NBD are then determined as

$$p = \frac{1}{1+s_{\rm I}^2\mu} \,, r = \frac{1}{s_{\rm I}^2}. \qquad (5)$$

In Figure 4, we show the distribution of subhalo number count of MW-mass hosts in three different subhalo mass bins, which are noted in each panel. In agreement with previous studies, we also find that the NBD describes the subhalo number count distribution much better than the Poisson distribution. Boylan-Kolchin et al. (2010) found that $s_{\rm I} \approx 0.18$ yields a good fit to the subhalo mass function distribution predicted by the Millennium-II Simulation. We find, however, a larger value for $s_{\rm I}$ is needed to describe the distribution. In the figure, we use $s_{\rm I} = 0.26$. When the expected number counts becomes smaller ($\bar{N} < 4$), the NBD approaches to the Poisson distribution, making it hard to distinguish between the two models. We also show the satellite galaxy number count distribution at three different stellar masses. As with the subhalo mass function distribution, the number count distribution for given stellar mass bin can also be accurately described by the NBD. Busha et al. (2011a) found that adding an exponential tail to the NBD can better capture the distribution at very high

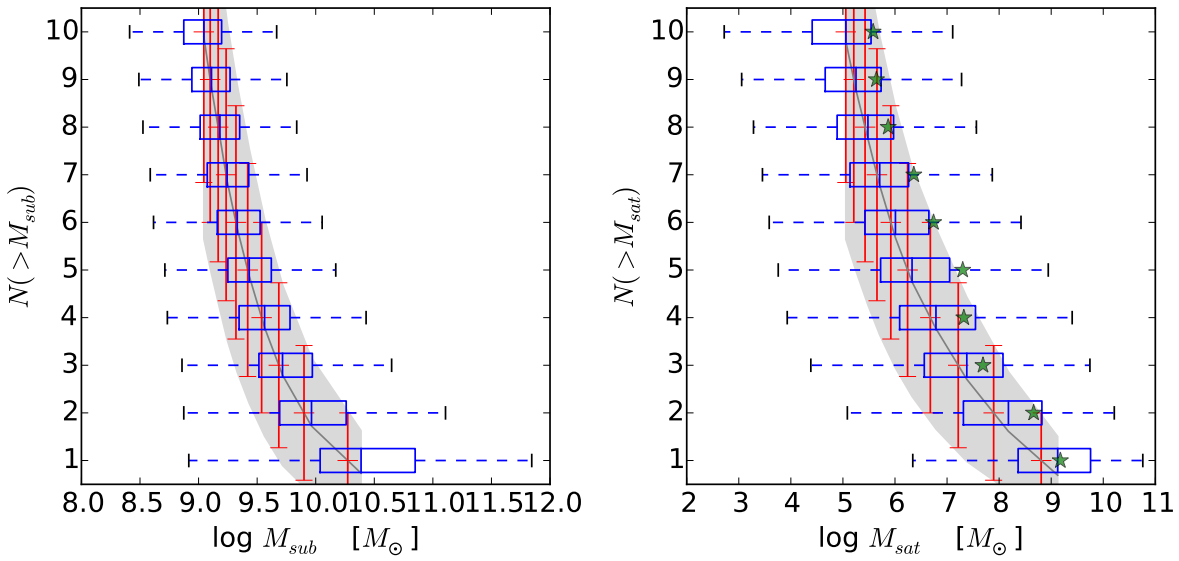

FIG. 3.— The left shows the sub-halo mass function of the MW host halos in the c125-2048 simulation. The right shows the satellite stellar mass function predicted by the fiducial SAM using the merger trees of the MW host halos in the c125-2048 simulation. In each panel, the horizontal whiskers show the distribution of the mass of the subhalo mass (or stellar mass) of the ith most massive subhalo (or satellite). The size of the box shows the quartiles of the distribution. The vertical bar in the middle of the box marks the median of the distribution in mass. The outer bars connected by dashed lines extend to the most extreme values. The red error bars show the standard deviation in the mass functions assuming the distribution of the mass functions follows a Poisson distribution. The gray shaded region shows the 1-σ range of the simulation (SAM) predicted mass function function. The dark gray line in the middle of the shaded region denotes the median of the distribution. In the satellite mass function panel (right), the green stars show the observational data of the stellar masses of the most massive MW satellite in stellar mass.

N. Because the tail only covers a small fraction of the probability distribution, we ignore this part for keeping the model simple without losing accuracy above the level our MCMC can capture.

Using the fiducial SAM, we predict the stellar mass for the satellite galaxies and compute the stellar mass function for each MW host. We show the distribution of the number of satellite galaxies in three stellar mass bins in the lower panel of Figure 4. Again, we use $s_{\rm I} = 0.26$ for the NBD plotted in the figure to compare with the model predictions and find that the NBD matches the simulated distribution of the stellar mass function remarkably well. We note that the value of the intrinsic scatter $s_{\rm I}$ can depend on galaxy formation model. In principle, the distribution can be simulated each time for a given model if a large number of merger trees are adopted. Limited by computation, we take $s_{\rm I}$ as a nuisance parameter to be sampled by MCMC in our study. We then marginalize the posterior distribution of $s_{\rm I}$ in subsequent analysis.

We have visually inspected the probability distribution of the MW subhalo mass function and the satellite mass function. We now quantitatively test which distribution function better matches the moments of the simulation predicted distribution of the mass functions. Using the large sample provided by the low-resolution simulations, we compute the 2-4th order moments of the subhalo mass function and the stellar mass function for given mass bins. Each sample contains 1133 MW halos. The simulation predicted moments for the subhalo mass function and the stellar mass function are shown in the upper panels and the lower panels of Figure 5, respectively. The moments monotonically increase with decreasing masses. Based on the hypothesis that the distribution function is Poisson or NBD, we generate same number of Monte Carlo mass functions, assuming each mass function is a random realization of the assumed distribution function. We adopt the simulation predicted means to assign the expected value for the Monte Carlo mass functions. Using the Monte Carlo mass functions, we can compute the same moments for the given mass bin. We then replicate the Monte Carlo simulation for 10000 times to obtain 10000 samples of the moments for each mass bin. We used these 10000 values to construct a reference distribution for each moment. In Figure 5 we show the distribution of the Monte Carlo subhalo mass function and satellite stellar mass function assuming the samples are Poisson distributed (red) or NBD (yellow). As one can see, the simulation predicted moments are largely deviated from the Poisson distribution, especially in the low-mass bins. The Monte Carlo simulations suggests that while the simulation predicted distribution is still consistent with Poisson at high-mass bins, it is clearly inconsistent with Poisson for low mass bins. In contrast, the NBD moments matches the moments of the simulated mass functions remarkable well. Supported by these tests, we adopt the NBD as the model for the likelihood function of the satellite stellar mass function.

3. RESULTS

3.1. *LMC/SMC and halo mass assembly history*

We now study what causes a MW mass host to have a high-mass satellite galaxy, similar to LMC and SMC. In Figure 6, we show the correlation between the mass of a satellite galaxy and its host subhalo property of 38 MW systems. We show the correlations for the first massive satellite in the left column and the second massive satel-

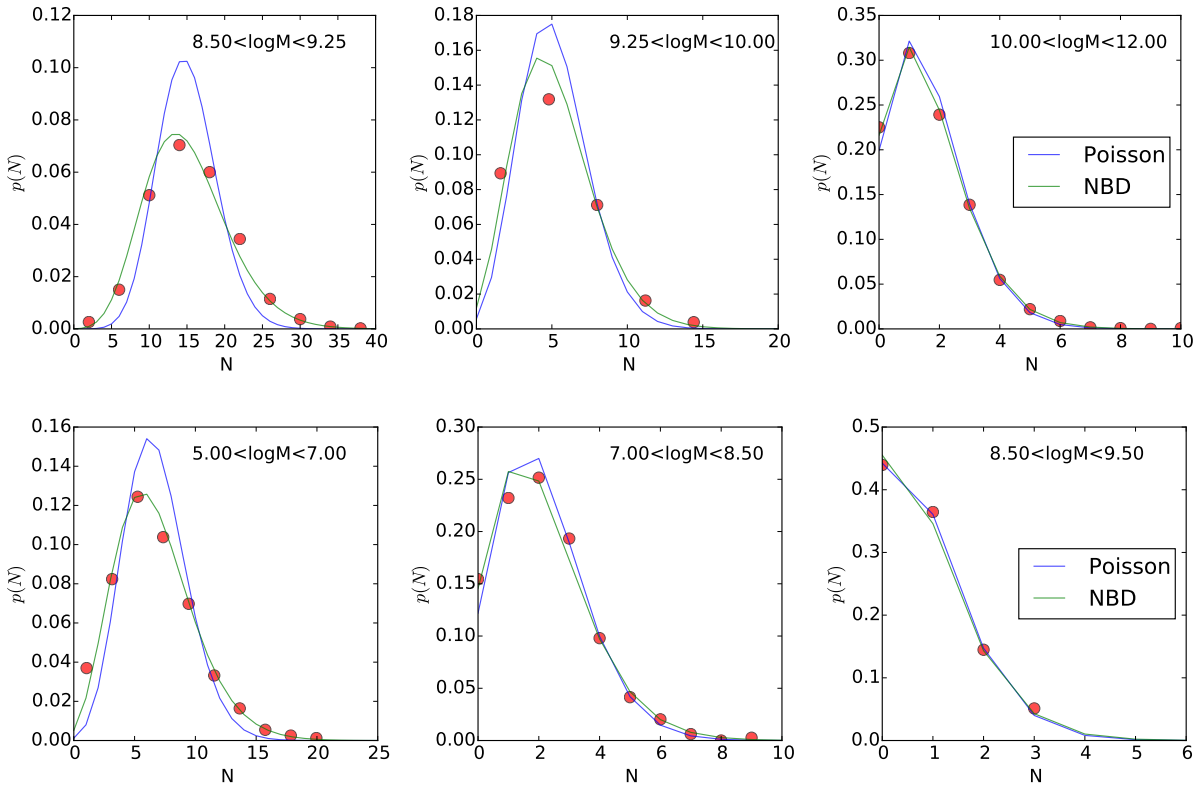

FIG. 4.— Upper: the distribution of the number of subhalos in three mass bins. Lower: the distribution of the number of satellites in three stellar mass bins. In each panel, the red circles denote the distribution of subhalo mass function (satellite stellar mass function) predicted by the low-res MW host simulations (and SAM applied to the merger trees). The blue line and the green lines show the Poisson distribution and negative binomial distribution with the same mean as the simulation predicted, respectively. For the negative binomial distribution, we have assumed $s_{\rm I} = 0.26$.

lite in the right column. The x-axis denotes the SAM predicted stellar mass for the satellites. For a given galaxy formation model, the most massive satellite in each host halo has very different stellar mass. In some systems, the most massive satellite can have a stellar mass higher than $10^{10}{\rm M}_{\odot}$, while in some other systems, the most massive satellite has a very low mass, $\sim 10^{5}{\rm M}_{\odot}$. The question is then what causes the big difference.

In the first row of Figure 6, we show the correlation between the stellar mass of the satellites and their final subhalo mass. It is clear that the galaxy mass is correlated with the host subhalo mass with a substantial scatter. Higher mass subhalos tend to host a high mass satellite, but for a given stellar mass, the scatter of the host subhalo mass is about a dex. We track the merger history of the subhalos and find the halo mass at the time when it is first accreted into another halo. In the middle panel, we show the halo mass at accretion as a function of the final stellar mass of those satellites. The correlation between the two quantities is even stronger, with a smaller scatter. This suggests that the halo mass at accretion is a better predictor of the final stellar mass of massive satellites. The third row shows the effect of model on the stellar mass of massive satellites. We vary the model parameters by a large amount from the fiducial model, and call this test model M1. The parameter set is off from the fiducial model and is outside the 95% posterior of the model constrained by the field stellar mass function (Lu et al. 2014). While the model predicts a different stellar mass for each subhalo, the rank order of the systems based on their massive satellite stellar mass does not generally change. What this means is that a system that is predicted to host a high mass satellite galaxy by an arbitrary model will also host a relatively high mass satellite if the galaxy formation physics is changed systematically for all galaxies.

Given that the final stellar mass of massive satellite galaxies are correlated with instantaneous subhalo mass, we further explore what host halo properties are correlated with suhhalo mass. In Figure 7, we show the distribution of all the simulated MW host halos in the parameter space defined by the MAH fitting parameters, $\beta+\gamma$ and γ. All the halos populate a particular region of the parameter space with a concentration around $\beta+\gamma = 0.3$ and $\gamma = 0.7$. This distribution is in agreement with what is found in other simulations (McBride et al. 2009; Taylor 2011). Different from other authors, we choose to use $\beta+\gamma$ as one of the axises for its physical meaning. In the diagram, halos in the upper left branch have rapid late time accretion, while those in the lower right branch have rapid early time accretion. We also note that when $\beta = 0$, the fitting model is exactly an exponential form and reduces to the Wechsler et al. (2002) model. The model that is occupied by a large population of halos is not too far from an exponential form. These halos do not belong to the populations that have extremely high rate of accretion at late or early times among the entire

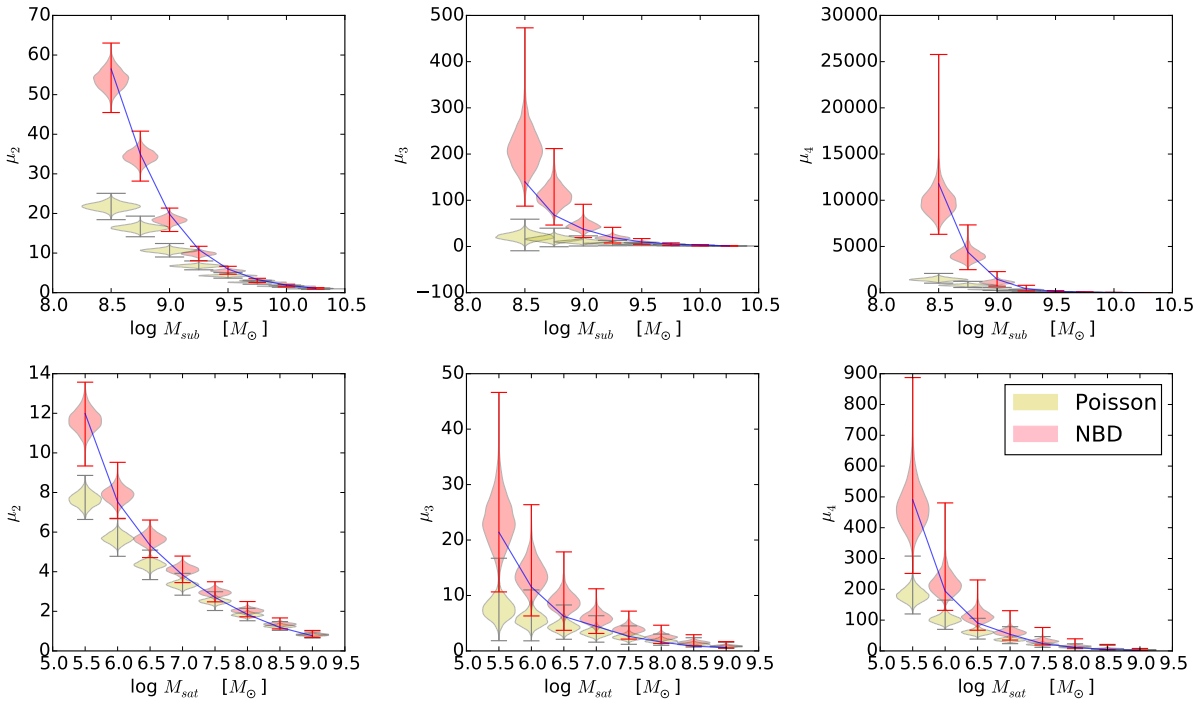

FIG. 5.— The 2nd, 3rd, and 4th moments of the distribution of subhalo and satellite mass functions as a function of mass. The blue line denotes the moments predicted by MW halos of the low-resolution simulation. The yellow shapes denote the reference distributions of the moments as a function of mass assuming that the mass functions are Poisson distributed. The red shapes denote the same reference distributions assuming that the mass functions follow the NBD. The simulation predicted mass functions have moments that are largely deviated from Poisson, especially for low masses, but consistent with the NBD.

population.

We fit the mass profile with a NFW model (Navarro et al. 1997) and use the size of the symbol to denote the characteristic core size of the halo. The size of the circle is linearly proportional to r_s and inversely proportional to the concentration parameter $c = R_{\rm vir}/r_s$. One can find that the r_s and concentration are closely correlated with the fitting parameters of the MAH. In general, halos with faster late-time accretion tend to have lower concentration (and larger r_s for given $R_{\rm vir}$). This result is in agreement with findings of Wechsler et al. (2002); Bullock et al. (2001); Zhao et al. (2003) and explained by models (e.g. Lu et al. 2006).

We also color code each halo according to the mass of the most massive subhalo hosted. Interestingly, the mass of the most massive subhalo is also correlated with the MAH parameters and the concentration of the host. Hosts that have higher accretion rate at late times and lower concentration (larger r_s for given $R_{\rm vir}$) tend to host high mass subhalos. Motivated by this finding, we plot the distribution of host halos in a diagram defined by halo concentration and $\beta + \gamma$ in the right panel of Figure 7. Using the same color coding, we find a clear sequence that halos with higher $\beta + \gamma$, indicating a higher recent accretion rate, have lower concentration and tend to host a higher mass subhalo. We define a division line in the $c - \beta + \gamma$ diagram to split simulated hosts into two groups. Halos in the lower-right corner have higher concentration and slower recent accretion, and their most massive subhalo typically have higher masses. Halos in the upper-left have lower concentration and faster recent accretion, and tend to host a high mass subhalo. We use a division line, which is shown by a dashed in in the right-panel of Figure 7, to split the halo samples into two groups. We name halos in the upper-left part of the diagram Group 1 halos, which are less concentrated, have more rapid recent accretion, and tend to host high-mass subhalos. We name halos in the lower-right part of the diagram Group 2 halos, which are more concentrated, have slower recent accretion, and do not tend to host high-mass subhalos. The division is defined here to roughly split the entire high-resolution host halos into two subsamples with equal size, likewise the low-resolution host halos. For the high-resolution hosts, we have 20 halos in Group 1, and 18 halos in Group 2.

For each group, we show the general trend of the MAH and the concentration of the host halo as functions of redshift in Figure 8. We show the $1-\sigma$ range of the distribution of these functions predicted by the low-resolution simulation halos with the shaded region, and overplot 5 randomly selected high-resolution simulation halos in each category with solid lines. The Group 1 hosts have relatively more rapid mass accretion at late time ($z < 1$), while the Group 2 hosts have flat mass accretion history at late time. The concentration shows clear difference between the two groups. Group 1 hosts evolve their concentration slowly, but the Group 2 host increase their concentration rapidly at late time. The $1-\sigma$ range of the concentration for both groups stay round 5 from high redshift until $z \sim 1$ for both halo groups. Group 1 halos slowly increase their concentration, with the $1-\sigma$ range around 5-10 at $z = 0$. In contrast, Group 2 halos increase their concentration rapidly. At $z = 0$, the $1-\sigma$ range is between 10 and 15. We also show the

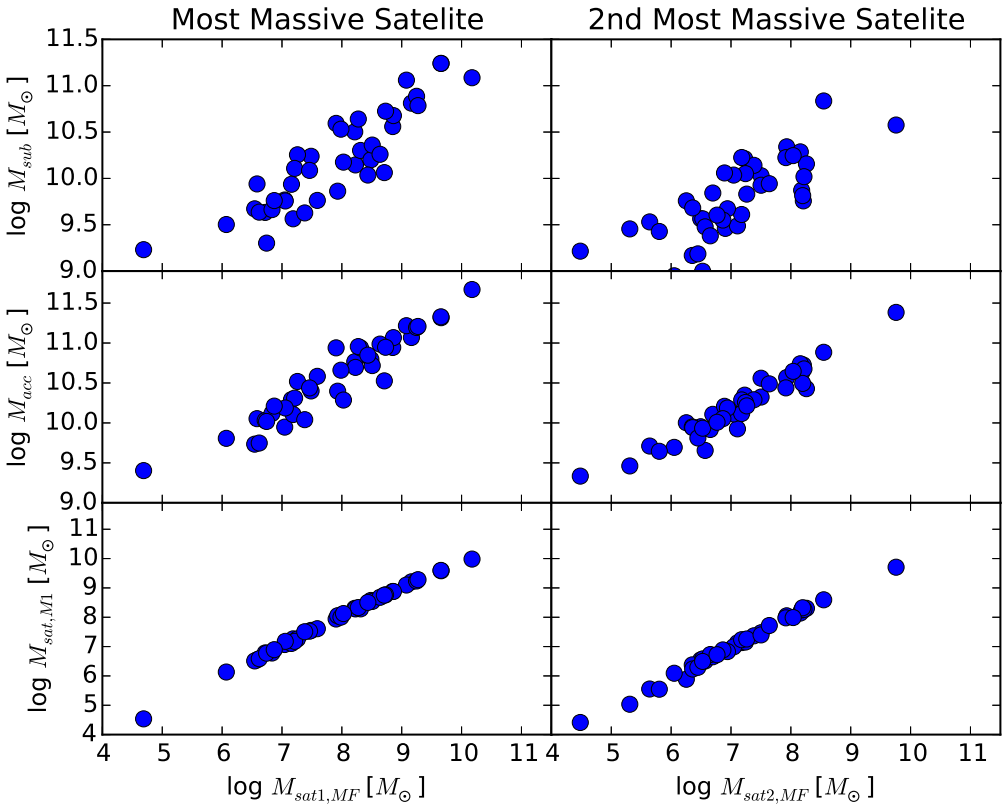

FIG. 6.— The first row shows the correlation between the final subhalo mass and the stellar mass of satellite galaxies predicted by the fiducial SAM. The second row shows the correlation between the halo mass at accretion and the final stellar mass. The third row shows the correlation between the stellar mass predicted by another model and the fiducial model. We show these correlations for the most massive satellite galaxy in each MW host in the first column, and the second massive satellite galaxies in the second column.

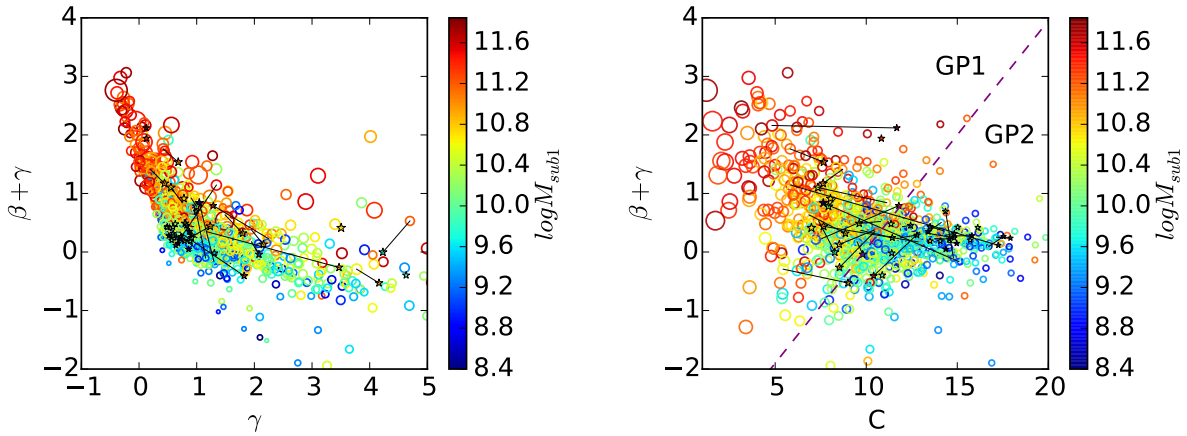

FIG. 7.— The distributions of the simulated MW hosts in parameter space. The left panel show the distribution of the host halo mass accretion history fitting parameters. The parameter γ indicates the early accretion rate, and $\beta+\gamma$ indicates the late accretion rate. The distribution has a mode peaks at $\gamma = 0.8$, $\beta+\gamma = 0.3$. Each circle represents a MW host from the low-resolution c125-2048 simulation and each star represents a high-res MW host. The right panel shows the concentration parameter versus $\beta+\gamma$. The color represents the mass of the most massive subhalo hosted by each MW host halo, indicated in the color bar. The size of each symbol is proportional to the size of NFW core radius r_s (or inversely proportional to the halo concentration parameter, C). The black solid lines in each panel connect the counterpart halos in the low-res and the high-res simulations. The purple dashed line in the right panel splits the distribution into two parts. Halos in the upper-left corner have lower concentration, and higher recent accretion rate, and their most massive subhalo typically has higher mass.

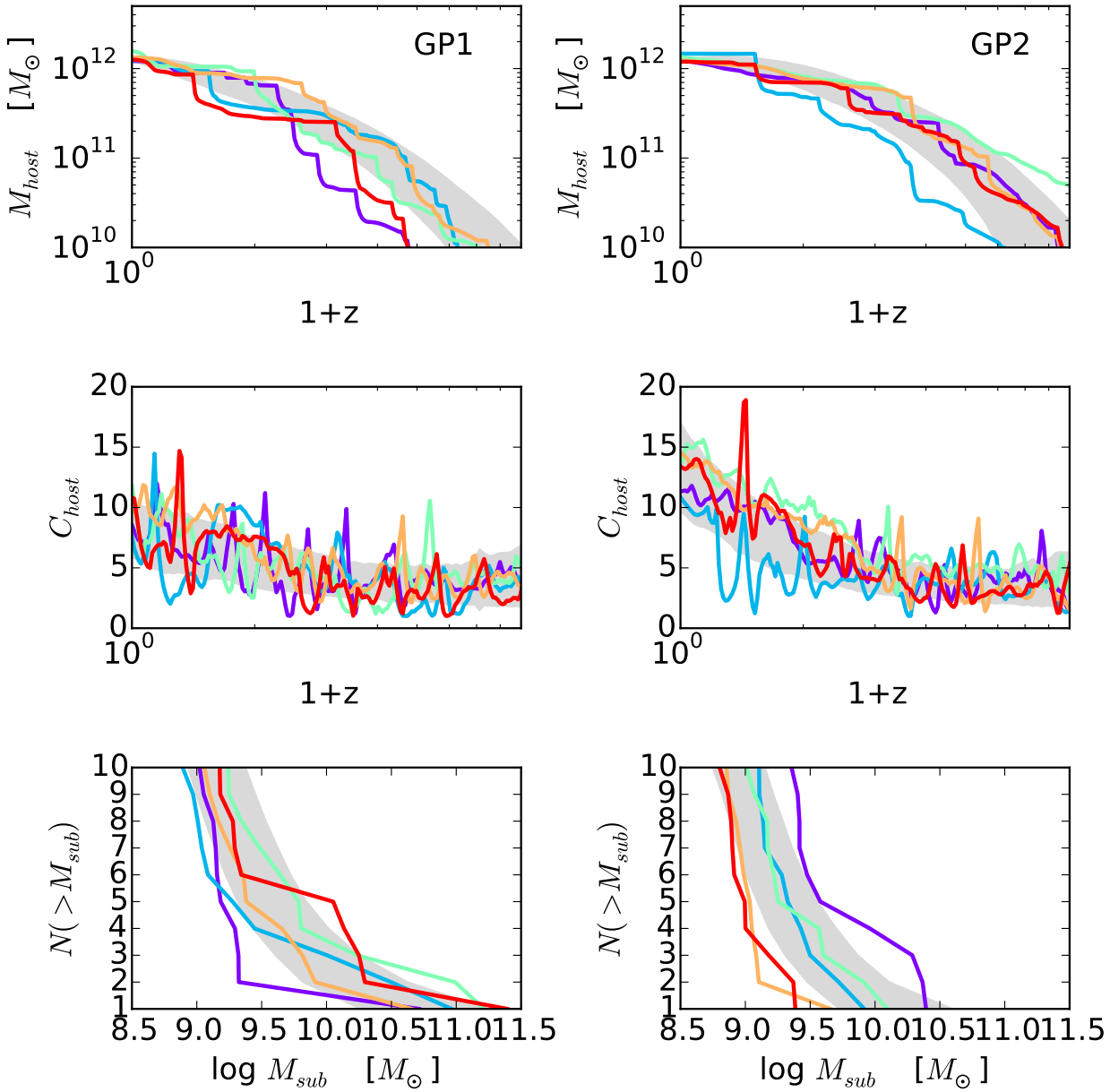

FIG. 8.— The host MAHs (upper), the evolution of concentration (middle), and the subhalo mass function (lower) predicted by the simulations. The shaded region denotes the $1-\sigma$ range of the distribution predicted by the low-res sample, and the thick lines denote 5 random samples from the zoom-in simulations. The left and right columns are for the Group 1 and Group 2 hosts.

subhalo mass function for each of the two halo groups in the figure. Although the low-mass part of the mass functions are quite similar, the high-mass part, the massive subhalo, show clear difference. The Group 1 hosts has significantly higher subhalos than the Group 2 hosts.

3.2. *Satellite galaxy stellar mass function*

We have classified simulated MW halos into two categories based on their concentration and formation history. Based on our classification, the whole high-resolution sample is split into two subsamples with roughly equal sizes. We stress that we do not have clear prior knowledge about which type of underlying dark matter halo the MW host halo belongs to. One can argue that the high stellar masses of LMC and SMC indicate high-subhalo masses, so the MW host is presumably Group 1 type. Direct observational constraints for the subhalo mass of LMC and SMC are needed to make conclusive answer. Theoretically, it is possible that the MW host halo belongs to Group 2, where the dark matter mass of the LMC and SMC subhalos are relatively low. The uncertainties in galaxy formation model is large enough to vary the ratio between stellar mass and subhalo mass. Nevertheless, we expect that host halos with different subhalo masses would require different star formation efficiency and feedback strength to produce certain amount of stellar mass to match observation. To test how the halo prior affects the inference of galaxy formation physics, we use the two halo groups as two explicit prior constraints to perform Bayesian inference from the MW satellite stellar mass function.

We adopt the stellar masses and memberships of MW satellite galaxies compiled in McConnachie (2012). We utilize the likelihood function we defined based on the NBD in Sec.2.3,

$$L(D|\theta) = \Pi_i P(N_i|r,p_i) = \Pi_i \frac{\Gamma(N_i+r)}{\Gamma(r)\Gamma(N_i+1)} p_i^r (1-p_i)_i^N \,, \tag{6}$$

where N_i is the number of satellite galaxies for a given stellar mass bin i per MW halo; the two parameters r and p are determined as $r = \frac{1}{s_{\rm I}^2}$, $p_i = \frac{1}{1+s_{\rm I}^2\mu_i}$; μ_i is the expected number for the i^{th} mass bin predicted by the model. We treat the fractional intrinsic scatter, $s_{\rm I}$, as a nuisance parameter to be sampled with MCMC because the limited number of merger trees are not enough to yield an accurate estimate for this parameter. Again, we only include the 11 most massive satellite galaxies into likelihood evaluation to best use the constraining power of the data while avoiding incompleteness, which becomes severe in lower masses. We use MCMC to sample the posterior probability density distribution. Two separate runs are performed with Group 1 host halos and Group 2 host halos, respectively. In both runs, we allow six model parameters and the nuisance parameter $s_{\rm I}$ to vary within their prior range. These model parameters are Σ, which is threshold gas surface density for star formation in units of $\rm M_\odot pc^{-2}$, $\alpha_{\rm LD}$ the normalization of mass-loading factor for feedback outflow, $\beta_{\rm LD}$ the power index for the circular velocity dependence of the mass-loading factor, $V_{\rm out}$ a characteristic halo circular velocity in km/s, below which all outflow mass leaves the host halo, $\beta_{\rm out}$ the steepness of the transition from total outflow for halos with $V_c < V_{\rm out}$ to no outflow for halos with $V_c > V_{\rm out}$, and $\gamma_{\rm RI}$ the rate for the outflow mass to reincorporate back into the halo. For detailed explanation of these parameters, readers are referred to Lu et al. (2014). The parameters, $\beta_{\rm LD}$, $\beta_{\rm out}$, and $S_{\rm I}$ are given uniform priors in linear scale, and Σ, $\alpha_{\rm LD}$, $\gamma_{\rm RI}$ are assigned uniform priors in logarithmic scale. The ranges of the priors are shown in Figure 9. For each run, we run the MCMC for 20,000 iterations with 144 parallel chains using the differential evolution algorithm (Ter Braak 2006). The convergence test is done with the Gelman-Rubin test (Gelman & Rubin 1992), requiring $\hat{R} < 1.2$. After removing outliers and pre-turn-in states, we obtain 2,000,000 posterior samples from the MCMC. For these runs, the "best fit" model (maximum likelihood) is close to the median model of the full posterior.

We show the 2-D marginalized posterior distribution for the Group 1 run and the Group 2 run in Figure 9. As one can see, under the same data constraints, using different halo prior results in different posteriors of the model parameters. An obvious change is that the normalization and the power index for the parameterization of the the mass-loading factor of outflow. In the model, the outflow mass-loading factor is parameterized as

$$\eta = \alpha_{\rm LD} \left(\frac{V_{\rm c}}{220{\rm km/s}} \right)^{-\beta_{\rm LD}} , \tag{7}$$

where $V_{\rm c}$ is the circular velocity of a halo, $\alpha_{\rm LD}$ and $\beta_{\rm LD}$ are model parameters to be constrained. The normalization parameter $\alpha_{\rm LD}$ for Group 1 is higher than that for Group 2. Correspondingly, the power index for Group 1 is lower than that for Group 2. The normalization for the mass-loading factor is defined as the mass-loading factor for halos with a circular velocity $V_c = 220$km/s. This parameter directly represents the strength of SN feedback driven outflow. A higher α requires a higher fraction of SN energy to power outflows to keep the baryon fraction of a halo low. The Group 1 halos are those having high probability to host massive subhalos. The high-mass subhalos typically have higher baryon mass to start with before being accreted into the host. To keep the baryon mass fraction low in those high-mass subhalos, the model is required to have stronger feedback to suppress star formation. The Group 2 halos, which do not tend to have massive subhalos, typically require lower feedback to allow relatively higher stellar mass fraction to fit the satellite mass function.

It is clear that the two parameters for outflow mass-loading factor are strongly degenerate, regardless of which halo prior is adopted. The degeneracy can be described by a linear function as $\beta_{\rm LD} = A \log \alpha_{\rm LD} + B$, where A and B are the slope and the intercept of the linear function. The straight line in Figure 10 captures the slope and intercept, with $A = -1.2$ and $B = 4$. Recall that the outflow mass-loading factor is parameterized as Eq. 7. One finds that in order to have any combination of $\alpha_{\rm LD}$ and $\beta_{\rm LD}$ to exactly follow a linear function defined by fixed A and B, the following condition needs to be fulfilled. The condition is when $\log V_{220} = \frac{1}{A}$, $\log \eta = -\frac{B}{A}$. For degeneracy found in this work, we find that the outflow mass-loading factor models have $\eta \approx 2100$, when $V_{\rm c} = 32$km/s. This is the generic feature for all models that are on the ridge of the degeneracy. This velocity

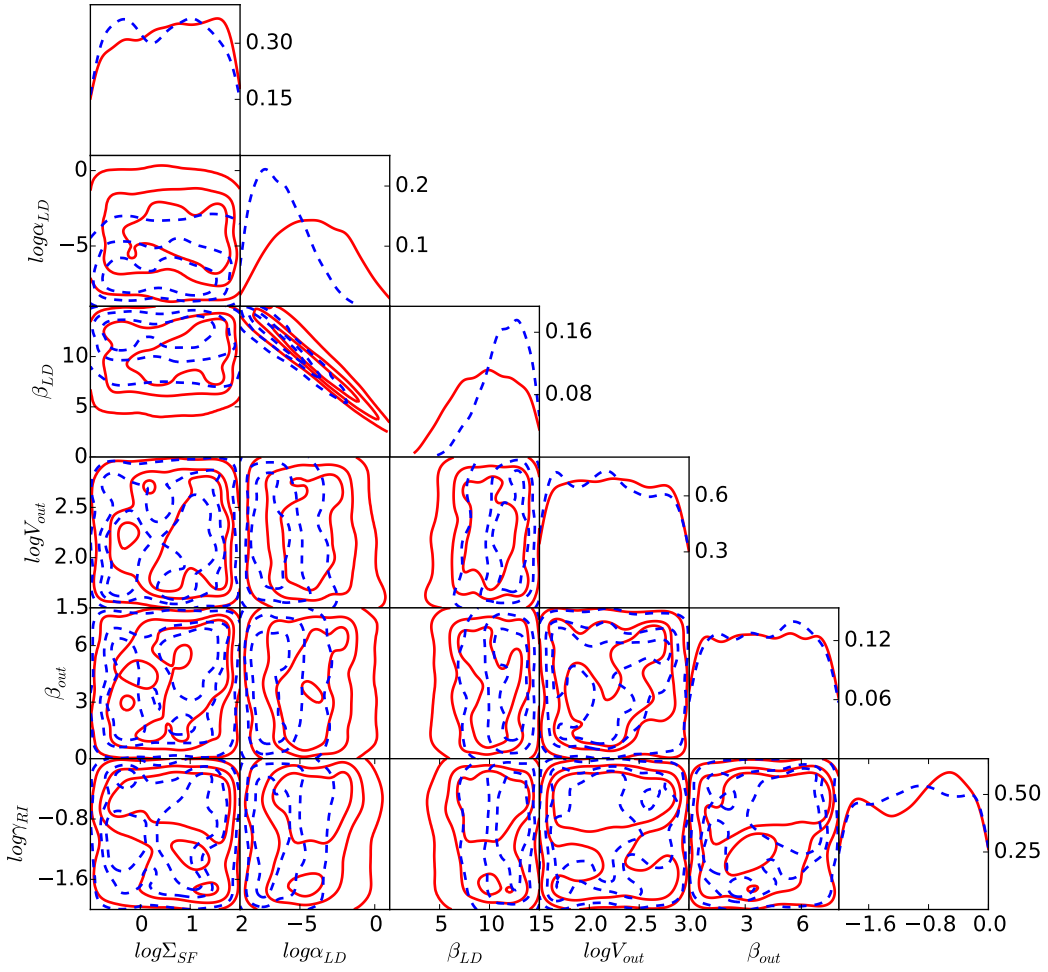

FIG. 9.— Posterior probability distributions of the SAM parameters constrained with the MW satellite stellar mass function. The red-solid contours denote the posterior distribution derived using the Group 1 merger trees, and the blue-dashed contours denote the distribution using the Group 2 merger trees.

scale is interesting because it is between the circular velocity of SMC and less massive satellites, Canis Major and Sagittarius dSph and so on. The degenerate models collectively require extremely high outflow mass-loading factor for subhalos with circular velocity as low as (or lower than) 32 km/s. It would be interesting to investigate the significance of this velocity scale using other data sets of the galaxy population.

We marginalize the posterior to show how the model, together with its predetermined halo prior, reproduces the MW satellite stellar mass function. The reproduced stellar mass function using the two underlying dark matter halo priors are shown in Figure 11. The red bands denote the posterior predictive distribution using the Group 1 halo prior. The solid line in the middle of the bands denotes the median of the predictive distribution, and the bands from darker to lighter color enclose 20%, 50%, and 80% of the predictive probability distribution. Similarly, the blue bands show the predictive distribution using the Group 2 halo prior with three levels of color darkness. In addition, we also show the observed satellite mass function of the MW in the same figure. We find that when the model applied to Group 1 host, it can achieve very good match to the observed stellar mass function for the most massive 11 satellite galaxies. When the model is applied to Group 2 hosts, while the model matches the mass function equally well as using Group 1 host for satellites with mass lower than SMC, it still tends to predict lower stellar masses for the 2 most massive satellite galaxies. It is because the hosts do not host high-mass subhalos, precluding the solutions for making high enough mass to match the high-mass satellite galaxies. We compute the marginalized likelihood for each of the inference using different halo priors. The Bayes Factor, which is defined as the ratio between the marginalized likelihood of the model based on the Group 1 halo prior and the marginalized likelihood of the model based on the Group 2 halo prior. We find

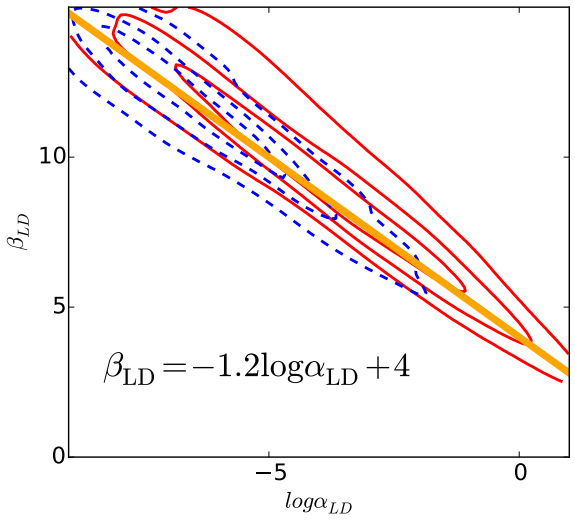

FIG. 10.— The red contours denote the posterior for the feedback outflow mass-loading parameters using the Group 1 halo prior. The blue contours denote the posterior for the same parameters of the model using the Group 2 halo prior. The solid linear line, $\beta_{\rm LD} = -1.2 \log \alpha_{\rm LD} + 4$ captures the degeneracy between the two model parameters in both runs.

that the Bayes Factor $\mathcal{B} = \frac{\mathcal{M}_1}{\mathcal{M}_2} = 1.42$, which indicates that the halo prior of Group 1 type MW host is only weakly preferred by the data over the halo prior of Group 2 type host. Due to large uncertainties, the model is not able to distinguish between the two types of underlying dark matter halo using the observed MW satellite galaxy stellar mass function. Further inferences involving more data are needed.

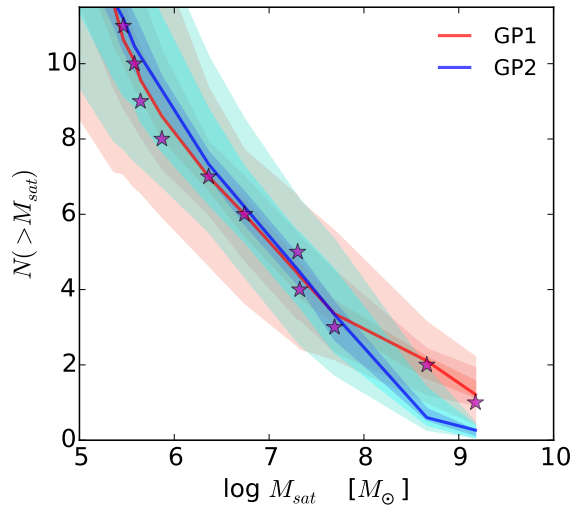

FIG. 11.— The posterior predictive distribution of the MW satellite stellar mass function. The red is predicted by the model constrained using host halo group 1, and the blue is predicted by the model constrained using host halo group 2. The bands with decreasing intensity are the 20%, 50%, and 80% predictive distribution for each halo group. Observational data from (McConnachie 2012) are shown by star symbols.

3.3. *Metallicity relation of MW satellites*

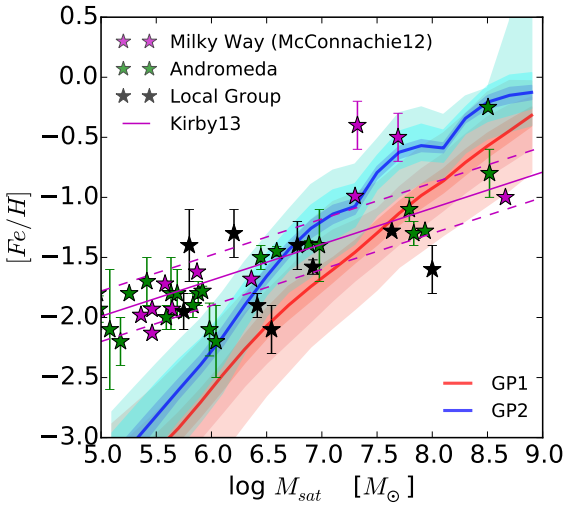

FIG. 12.— The posterior predictive distribution of the stellar-phase metallicity as a function of stellar mass. The red is predicted by the model constrained using host halo group 1, and the blue is predicted by the model constrained using host halo group 2. Observational data from (McConnachie 2012) for different populations are shown by star symbols.

We now make predictions for the stellar-phase metallicity as a function of stellar mass for the MW satellite galaxies based on the two halo priors and the corresponding models specifically tuned for the halo prior. Instead of choosing one single model (the best or any arbitrary one), we use the posterior samples obtained with MCMC to produce the posterior predictive distribution Lu et al. (2012). The predictive distribution marginalizes over the model uncertainties that are allowed by the uncertainties of the constraining data, and quantifies the confidence levels of the predictions for the given model and prior. The posterior predictive distributions for both host halo priors are shown in Figure 12. In the figure, the red bands are predicted using the posterior constrained for the Group 1 halo prior, and the blue bands are predictions using the posterior constrained with the Group 2 halo prior. The bands with different intensity of each color show the 20%, 50%, and 80% predictive distribution. We find that while the model can be tuned to reproduce the satellite stellar mass function using either halo prior, they make rather different predictions for the stellar-phase metallicity-stellar mass relation. For the Group 2 prior, because the hosts typically do not have high-mass subhalos, the model needs weaker feedback and outflow to yield a relatively higher stellar mass for given subhalo mass. The consequence of the weaker outflow is to leave more metals in the galaxies, resulting in a higher metallicity for given stellar mass. In contrast, the Group 1 prior imposes host halos that typically host high-mass subhalos. The high-mass subhalos require higher outflow, which take away metals with hydrogen masses from the galaxy. The result suggests that for given galaxy formation scenario, when it is calibrated to the stellar mass function, the properties of the under-

lying dark matter halo, including the formation history, concentration and subhalo masses, can leave imprints in the satellite galaxy metallicity relation. Because the high-mass end of the subhalo mass function is correlated with the host formation history and concentration, the metallicity may also reflect the formation and structure properties of the host halo of the MW and its analogues.

3.4. *Satellites accreted with LMC*

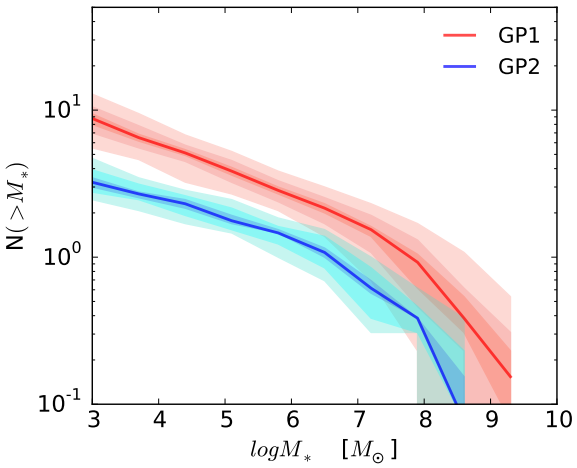

FIG. 13.— The posterior predictive distribution of the cumulative mass function of satellite galaxies that are accreted into MW host halo in a same halo of the most massive satellite galaxy. The red is predicted by the model constrained using host halo group 1, and the blue is predicted by the model constrained using host halo group 2.

In a CDM cosmology, the higher amplitude of power spectrum at small scales gives rise to a large number of substructures in a halo (e.g. Kravtsov et al. 2004b). We explore the number of satellites galaxies that are accreted into the MW host halo together with the LMC (or LMC/SMC common halo). These smaller halos were subhalos of the LMC/SMC hosts before accreted into the MW host. They may still stay gravitationally bound with the LMC/SMC host subhalo, or have been tidally stripped from the subhalo but live in the vicinity of the LMC/SMC. Using the models that are calibrated to match the satellite mass function using MCMC, we test if the satellite galaxies that are accreted with the LMC/SMC can provide information to discriminate the halo priors.

Using the SAM prediction and the merger tree, we identify the most massive satellite galaxy as "LMC" and track the host halo of the satellite galaxy. In the merger tree, we find its host halo when it is just accreted into the MW host. If the halo is accreted into the MW multiple times, we count the last time when it is accreted as the accretion time. We then track the history of all other galaxies hosted by the subhalo since this epoch and identify the ones that still exist at $z = 0$. We repeat this calculation for every model in a posterior sample to produce a posterior predictive distribution. In Figure 13, we show the stellar mass function of the satellite galaxies that are accreted into the MW host together with the LMC as predicted by the constrained models. The stellar masses are the final stellar mass predicted by the SAM. We show the stellar mass function of this population predicted using the two different host halo priors. One can find that the Group 1 hosts have systematically higher number of satellites that are accreted with LMC than the Group 2 hosts. The prediction shows that down to $10^3 M_\odot$, one would expect more than 10 satellite galaxies that are accreted with the LMC for the Group 1 hosts. If the MW host belongs to Group 2, one would expect the number satellite galaxies with stellar mass higher than $10^3 M_\odot$ that are accreted with LCM no more than a few. The reason is simple that the host subhalo of LMC in the Group hosts is typically higher than those of the Group 2 hosts. When they are accreted in the MW, their higher mass allow them to bring in more low-mass subhalos altogether. The result suggests that finding and identifying very low-mass satellite galaxies that are associated with LMC and SMC may provide very useful constraints on the LMC/SMC subhalo mass and the MW host prior.

4. DISCUSSION

In this paper, we analyze a suite of N-body cosmological simulations of Milky Way-sized halos. The analysis shows that the existence of high-mass subhalo is correlated with the formation history of the host halo and its concentration. For fixed halo mass, halos that have rapid recent accretion characterized by the fitting parameter $\beta + \gamma$ of the mass accretion history tend to host high-mass subhalo that are still exist at the present day. Those halos also tend to have lower concentration. The result suggests that the existence of LMC/SMC in the Milky Way halo indicates that the Milky Way is hosted by a dark matter halo that has lower concentration than average halos at the same mass. The formation history of the Milky Way halo may also have a particular shape, with significant accretion since $z = 1 \sim 0.5$. However, due to large uncertainties of galaxy formation model, we still cannot conclusively determine the properties of the MW host halo in terms of its concentration and formation history based on our inferences from solely the MW satellite galaxy stellar mass function.

The trends we find in the dark matter halo properties are still interesting. It has been known that the halo formation time is highly correlated with the concentration of the halo (Wechsler et al. 2002). Halos of same mass but different formation history can have very different characteristics or reside in different environments (e.g. Bullock et al. 2001; Allgood et al. 2006; Macciò et al. 2007). The differences in environment may give rise to different subhalo population that are recently accreted from the environment. For this reason, the abundance of subhalos within a dark matter halo does not only correlate with the mass of the halo (e.g. Kravtsov et al. 2004a) but also the formation history of the halo (e.g. Zentner et al. 2005; Zhu et al. 2006). For this reason, it is important to understand the properties other than the mass when we study the formation of the MW, because the structure of the host halo, formation history, and its substructures may contain critical information to tell the MW from other galaxies with similar masses.

In this paper, we explore the effect of the host halo prior, which is characterized by the recent MAH and concentration, on the inferences of the formation physics of

dwarf galaxies in the Milky Way. We find that when applying different host halo priors the observed stellar mass function requires different strength and circular velocity dependence for the feedback process. Although galaxy formation models are uncertain in accurately capturing how feedback works in detail, when the uncertainties of model parameters are marginalized, we find that host halos with rapid recent accretion require much stronger feedback than those without strong recent accretion. It is simple to understand because halos with significant recent accretion tend to host high-mass subhalos, which needs lower stellar mass to halo mass ratio to match the mass function.

We highlight that the different feedback strengths, according to the underlying dark matter halo, leave observable imprint in the mass-metallicity relation of dwarf galaxies. This is because outflow does not only suppress star formation but also expels produced metals out of galaxies. When the model requires stronger feedback, it inevitably results in lower metallicity in dwarf galaxies. The result indicates that if we understand how feedback works in galaxy formation, we can use the model to learn about the underlying dark matter halo formation history of the Milky Way by using observed metallicity relations. We stress, however, this requires accurate modeling of galaxy formation.

Moreover, we find that different halo priors predict different number of higher order satellite galaxies that are accreted into the MW together with high mass satellites, for example LMC, SMC, or their common halo. When constrained to reproduce the MW satellite galaxy stellar mass function, the host halos that have recent rapid accretion and lower concentration tend to host more satellites associated with the LMC. In contrast, hosts that have slow accretion lately and higher concentration have much lower number of high-order satellites, due to their lower subhalo mass of the LMC. The result suggests that finding and identifying low-mass satellite galaxies that are physically or historically associated with high-mass satellite may provide useful constraints on the property of the MW (Deason et al. 2015). The ongoing survey of low-mass satellite galaxies around the vicinity of the LMC/SMC (e.g. Bechtol et al. 2015; Drlica-Wagner et al. 2015) may provide more data for further theoretical investigation.

Our current understanding about galaxy formation is still poor. We have shown that the model, even with very large flexibility, does not readily reproduce the mass-metallicity relation when it is precisely constrained to the stellar mass function of the MW dwarfs. Based on the ejective feedback scenario, the model that matches the mass function is needed to have very large mass-loading factor for halos with circular velocity ~ 30km/s, but the model predicts perhaps too low metallicity for low-mass galaxies because much of the metal mass is lost in outflow. This problem seems to be general and regardless of which halo prior is adopted (Lu et al. 2014). In a future paper, we will study the constraining power of the metallicity relation of MW dwarf galaxies and to better understand the implication of star formation histories of Milky Way dwarf galaxies. The variations in the host halo formation history (reflected in the halo concentration and feedback strength) and their impact on star formation histories will be further studied. The star formation history of Milky Way dwarfs may also carry information about the formation history of the host halo.

ACKNOWLEDGEMENTS

REFERENCES

Allgood, B., Flores, R. A., Primack, J. R., et al. 2006, MNRAS, 367, 1781

Bechtol, K., Drlica-Wagner, A., Balbinot, E., et al. 2015, ApJ, 807, 50

Benson, A. J., Frenk, C. S., Lacey, C. G., Baugh, C. M., & Cole, S. 2002a, MNRAS, 333, 177

Benson, A. J., Lacey, C. G., Baugh, C. M., Cole, S., & Frenk, C. S. 2002b, MNRAS, 333, 156

Berlind, A. A., & Weinberg, D. H. 2002, ApJ, 575, 587

Boylan-Kolchin, M., Besla, G., & Hernquist, L. 2010, ArXiv e-prints, arXiv:1010.4797

Bullock, J. S., Kolatt, T. S., Sigad, Y., et al. 2001, MNRAS, 321, 559

Busha, M. T., Marshall, P. J., Wechsler, R. H., Klypin, A., & Primack, J. 2011a, ApJ, 743, 40

Busha, M. T., Wechsler, R. H., Behroozi, P. S., et al. 2011b, ApJ, 743, 117

Cautun, M., Frenk, C. S., van de Weygaert, R., Hellwing, W. A., & Jones, B. J. T. 2014a, MNRAS, 445, 2049

Cautun, M., Hellwing, W. A., van de Weygaert, R., et al. 2014b, MNRAS, 445, 1820

Deason, A. J., Wetzel, A. R., Garrison-Kimmel, S., & Belokurov, V. 2015, MNRAS, 453, 3568

Drlica-Wagner, A., Bechtol, K., Rykoff, E. S., et al. 2015, ApJ, 813, 109

Gelman, A., & Rubin, D. 1992, Statistical Science, 7, 457

Jiang, F., & van den Bosch, F. C. 2015, MNRAS, 453, 3575

Koposov, S. E., Yoo, J., Rix, H.-W., et al. 2009, ApJ, 696, 2179

Kravtsov, A. V., Berlind, A. A., Wechsler, R. H., et al. 2004a, ApJ, 609, 35

Kravtsov, A. V., Gnedin, O. Y., & Klypin, A. A. 2004b, ApJ, 609, 482

Lu, Y., Mo, H. J., Katz, N., & Weinberg, M. D. 2006, MNRAS, 368, 1931

—. 2012, MNRAS, 421, 1779

Lu, Y., Mo, H. J., Weinberg, M. D., & Katz, N. 2011, MNRAS, 416, 1949

Lu, Y., Wechsler, R. H., Somerville, R. S., et al. 2014, ApJ, 795, 123

Macciò, A. V., Dutton, A. A., van den Bosch, F. C., et al. 2007, MNRAS, 378, 55

Mao, Y.-Y., Williamson, M., & Wechsler, R. H. 2015, ApJ, 810, 21

McBride, J., Fakhouri, O., & Ma, C.-P. 2009, MNRAS, 398, 1858

McConnachie, A. W. 2012, AJ, 144, 4

Navarro, J. F., Frenk, C. S., & White, S. D. M. 1997, ApJ, 490, 493

Okamoto, T., Frenk, C. S., Jenkins, A., & Theuns, T. 2010, MNRAS, 406, 208

Springel, V., White, S. D. M., Jenkins, A., et al. 2005, Nature, 435, 629

Springel, V., Wang, J., Vogelsberger, M., et al. 2008, MNRAS, 391, 1685

Stanimirović, S., Staveley-Smith, L., & Jones, P. A. 2004, ApJ, 604, 176

Strigari, L. E., Bullock, J. S., Kaplinghat, M., et al. 2007, ApJ, 669, 676

Tasitsiomi, A., Kravtsov, A. V., Gottlöber, S., & Klypin, A. A. 2004, ApJ, 607, 125

Taylor, J. E. 2011, Advances in Astronomy, 2011, 6

Ter Braak, C. J. F. 2006, Stat. Comput., 16, 239

Tollerud, E. J., Bullock, J. S., Strigari, L. E., & Willman, B. 2008, ApJ, 688, 277
van den Bergh, S. 2000, The Galaxies of the Local Group (Cambridge)
van den Bosch, F. C. 2002, MNRAS, 331, 98
van der Marel, R. P., Alves, D. R., Hardy, E., & Suntzeff, N. B. 2002, AJ, 124, 2639
van der Marel, R. P., & Kallivayalil, N. 2014, ApJ, 781, 121
Wang, W., Han, J., Cooper, A. P., et al. 2015, MNRAS, 453, 377
Wechsler, R. H., Bullock, J. S., Primack, J. R., Kravtsov, A. V., & Dekel, A. 2002, ApJ, 568, 52
Zentner, A. R., Berlind, A. A., Bullock, J. S., Kravtsov, A. V., & Wechsler, R. H. 2005, ApJ, 624, 505
Zhao, D. H., Jing, Y. P., Mo, H. J., & Börner, G. 2003, ApJ, 597, L9
Zhu, G., Zheng, Z., Lin, W. P., et al. 2006, ApJ, 639, L5